# Nonparametric Reconstruction of Vector Fields From Noisy Observations of Their Flow Curves

Terry-Ann Sneed and Arash Komaee

Abstract—In an ordinary differential equation represented by a set of state-space equations, the differential of the state vector is given by the values of a vector feld evaluated at the values of the state vector. This paper focuses on the reconstruction of this vector feld from noisy measurements of the state trajectories generated empirically from a physical process. For this estimation problem, a nonparametric least squares formulation is presented, which is then expressed as a linear quadratic tracking problem with a well known solution from the optimal control theory. This approach is demonstrated for experimental reconstruction of the magnetic force feld around a permanent magnet from the motion trajectories of a magnetic particle attracted toward the magnet.

Index Terms—Least squares method, linear quadratic tracking, magnetic force, numerical differentiation, signal smoothing.

#### I. INTRODUCTION

THIS work aims to experimentally characterize magnetic force feld around a permanent magnet, and is part of our long-term effort toward a framework for systematic design and development of noncontact magnetic manipulators. Magnetic felds provide a unique ability for noncontact manipulation of magnetized objects behind nonmagnetic barriers, which can be exploited for operation of magnetically driven medical tools inside the human body, or for actuating micro- and nanoscale systems in which direct contact for manipulation and control is not feasible [1]–[20]. For effective design and feedback control of magnetic manipulators, a reliable model of magnetic force is an essential need. The existing models of magnetic force are usually theoretically driven, while empirical models are more reliable due to the existing gap between theory and practice.

In this work, a model of magnetic force is constructed from empirical data. An experimental setup was used to record the trajectories of motion of a magnetic particle attracted toward a permanent magnet. These trajectories are the f ow curves of the magnetic force, which can be processed to reconstruct this vector f eld. Ideally, a vector f eld can be constructed along its f ow curves simply by differentiating these curves with respect to time. However, the accuracy of this approach for empirical data is severely degraded by the measurement noise and limits on the maximum achievable sampling rate of the f ow curves.

To improve the estimation accuracy, a least squares problem is formulated in this paper to both smooth the empirical f ow curves and estimate their differentials. This formulation takes the form of a linear quadratic tracking (LQT) problem with an

This work was supported by the National Science Foundation under Grant ECCS-1941944.

The authors are with the School of Electrical, Computer, and Biomedical Engineering, Southern Illinois University, Carbondale, IL 62901, USA email: {terry-ann.sneed, akomaee}@siu.edu.

explicit solution known from the optimal control theory [21]. By solving this problem for each empirical f ow curve (noisy and sampled), the vector feld is constructed along that curve, and by gathering a large collection of these curves, the vector feld is interpolated at those points not lying on the curves.

Most of prior work on reconstruction of vector f elds focuses on two categories of problems differing from this paper either in terms of the structure of empirical data or the reconstruction approach. In tomographic reconstruction, the goal is to extract a vector f eld from a collection of its line integrals [22]–[28], versus the f ow curves used in this paper. The second research direction relies on parametric techniques for reconstruction of vector f elds [29]–[38], in opposition to this paper that adopts a nonparametric approach. The least squares estimation problem formulated in this paper can be similarly applied for smoothing any noisy trajectory of motion, as extensively studied in [39].

#### II. EXPERIMENTAL SETUP AND DATA COLLECTION

The experimental setup shown in Fig. 1(a) was used in this work for data collection. This setup consists of a f at container flled with a high viscosity fuid, and a magnetic bead moving inside the fuid under the attractive magnetic force of a magnet f xed at the edge of the container. A simple screw mechanism is embedded into the setup to adjust the container horizontally using a bubble level. A high-speed camera is mounted on the top of the container to record the trajectories of motion of the magnetic bead. The camera operates at a frame rate of 667 fps, and a LabVIEW video tracking module extracts the position of the magnetic bead from the captured frames. Certainly, the video tracker is imperfect and can only estimate the position with some error, regarded as a measurement noise. As shown in Fig. 1(c), several trajectories of the magnetic bead starting from different initial points were recoded using the setup of Fig. 1(a). Each recorded trajectory is stored as an array of the estimated positions and an array of their corresponding time stamps. The goal in this paper is to reconstruct the magnetic force around the magnet by processing the recorded data.

The motion of the magnetic bead is described by Newton's second law of motion under the applied magnetic force and the f uid resistance (drag). Let  $x(t) \in \mathbb{R}^2$  and  $v(t) \in \mathbb{R}^2$  denote, respectively, the position and velocity of the magnetic bead at time t in the planar coordinate system of Fig. 1(c). Then, the dynamics of the magnetic bead is governed by the state-space equations

$$\dot{x}\left(t\right) = v\left(t\right) \tag{1a}$$

$$\dot{v}(t) = -\frac{\mu}{m}v(t) + \frac{1}{m}F_{mag}(x(t)), \qquad (1b)$$

1

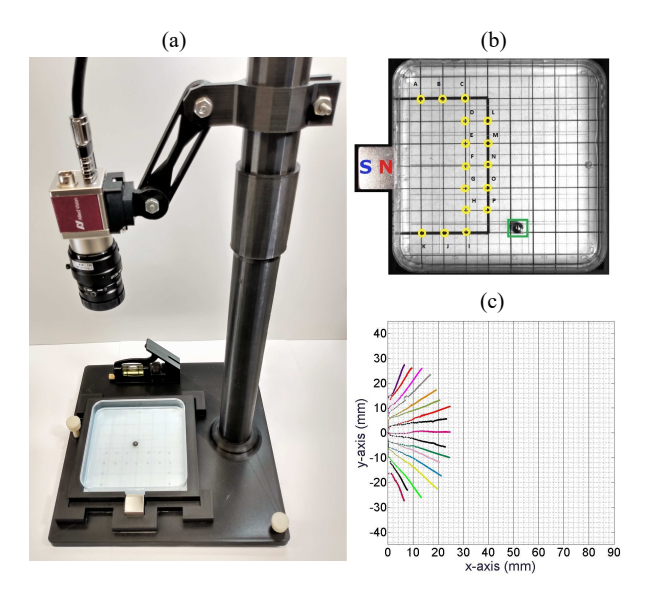


Fig. 1. Data collection procedure: (a) experimental setup consisting of a fat container f lled with a highly viscous fuid, a magnetic bead moving under a permanent magnet, and a camera on top for recording; (b) experimental set up as viewed by the camera; (c) recorded trajectories of the magnetic bead and the planar coordinate system in which they are represented.

where m is the mass of the magnetic bead. The term  $-\mu v\left(t\right)$  on the right-hand side of (1b) represents the drag force with the friction coeff cient  $\mu>0$ , linearly depending on the viscosity of the fuid surrounding the magnetic bead. Also,  $F_{mag}\left(x\right)$  on the right-hand side of (1b) characterizes the component of the magnetic force in the plane of motion at a point x.

The experiment in this work was purposefully designed with a high viscosity fuid aimed at two goals. First, the magnetic bead moves slower in a more viscous fuid, which enables the camera to capture more frames from each trajectory of motion. Second, for a high viscosity fuid with a very large  $\mu$ , the set of state-space equations (1) reduces to a single equation

$$\dot{x}\left(t\right) = \frac{1}{\mu} F_{mag}\left(x\left(t\right)\right)$$

by a singular perturbation [40] approximation  $\dot{v}\left(t\right)\simeq0$ . This reduced form is more convenient for the purpose of this paper, and is utilized to estimate the vector feld

$$f(x) \triangleq \frac{1}{\mu} F_{mag}(x) \tag{2}$$

from the recorded data. Then, by direct measurement of  $\mu$ , the actual magnetic force is obtained, or alternatively, the magnetic force is expressed in a normalized form, like this paper.

# III. RECONSTRUCTION OF VECTOR FIELDS

This section presents a solution to the inverse problem of reconstructing a vector feld from the noisy observations of its f ow curves. First, the problem is formalized in Section III-A, and next, a least squares formulation of the estimation problem is introduced in Section III-B. It is shown in Section III-D how this estimation problem can be converted to a linear quadratic tracking problem, for which an explicit solution is presented. Finally, a nearest neighbour interpolation scheme is presented in Section III-E to reconstruct the vector feld at those points not lying on any of the multiple reconstructed trajectories.

### A. Problem Statement

Let  $f(\cdot): \mathbb{R}^m \to \mathbb{R}^m$  be a continuous vector function and assume that the state-space equation

$$\dot{x}(t) = f(x(t)), \quad t \in [0, T] \tag{3a}$$

$$x\left(0\right) = x_0 \tag{3b}$$

admits a unique solution for the state vector  $x(t) \in \mathbb{R}^m$  on the interval  $t \in [0,T]$ , starting from the initial state  $x_0$ . Suppose the noisy observations

$$y_n = x(t_n) + v_n, \quad n = 0, 1, 2, \dots, N$$
 (4)

of the state vector are provided at the sampling times

$$0 = t_0 < t_1 < t_2 < \dots < t_N = T.$$

Here,  $v_n \in \mathbb{R}^m$ , n = 0, 1, 2, ..., N is a measurement noise of unspecified nature. The concern of this paper is to address the inverse problem of reconstructing the trajectories of x(t) and its derivative  $\dot{x}(t)$  on  $t \in [0, T]$  from the observed data (4).

The estimated trajectories are denoted by  $\hat{x}(t)$  and  $\hat{f}(\hat{x}(t))$ , respectively. These trajectories provide an estimate  $\hat{f}(\cdot)$  of the vector function  $f(\cdot)$  along  $\hat{x}(t)$ ,  $t \in [0,T]$ . By constructing several such estimated trajectories from different data sets of the form (4), the values of  $f(\cdot)$  can be estimated at the points not lying on the curves  $\hat{x}(t)$  by means of interpolation. This procedure is explained in Section III-E.

# B. Least Squares Formulation of the Estimation Problem

Perhaps, the simplest scheme for construction of  $\hat{x}(\cdot)$  at the sampling times  $t_n$  is to disregard noise and take  $\hat{x}(t_n) = y_n$  for  $n = 0, 1, 2, \ldots, N$ . Moreover,  $\hat{f}(y_n) = \dot{y}_n$  is estimated by numerical differentiation of the data set (4) according to

$$\dot{y}_n \triangleq \begin{cases} \frac{y_1 - y_0}{t_1 - t_0}, & n = 0\\ \frac{y_{n+1} - y_{n-1}}{t_{n+1} - t_{n-1}}, & n = 1, 2, \dots, N - 1\\ \frac{y_N - y_{N-1}}{t_N - t_{N-1}}, & n = N. \end{cases}$$
 (5)

However, this approach typically produces inaccurate results in the presence of noise, in particular for the differential  $\dot{y}_n$ . A less crucial but still important drawback of this simple scheme is that it can only provide estimations at the sampling times not the entire interval  $t \in [0, T]$ .

In this section, a least squares problem is formulated to yield a continuously differentiable estimate  $\hat{x}(t)$  on  $t \in [0,T]$  with a reasonably small second derivative, while staying reasonably close to the observed values  $y_n$  at the sampling times  $t_n$ . Then, the derivative of  $\hat{x}(t)$  is taken as  $\hat{f}(\hat{x}(t))$  for  $t \in [0,T]$ .

Let x(t) be a vector in  $\mathbb{R}^m$  with continuous first derivative and piecewise continuous second derivative on  $t \in [0, T]$ . In terms of x(t), define  $z(t) \in \mathbb{R}^{2m}$  and  $u(t) \in \mathbb{R}^m$  as

$$z\left(t\right)=\begin{bmatrix}x^{T}\left(t\right) & \dot{x}^{T}\left(t\right)\end{bmatrix}^{T}, \quad u\left(t\right)=\ddot{x}\left(t\right), \quad t\in\left[0,T\right].$$
 (6)

Then, x(t) can be expressed by the state-space equations

$$\dot{z}(t) = Az(t) + Bu(t) \tag{7a}$$

$$x\left(t\right) = Cz\left(t\right) \tag{7b}$$

with the parameters

$$A = \begin{bmatrix} 0_m & I_m \\ 0_m & 0_m \end{bmatrix}, \quad B = \begin{bmatrix} 0_m \\ I_m \end{bmatrix}, \quad C = \begin{bmatrix} I_m & 0_m \end{bmatrix},$$

where  $I_m$  and  $0_m$  denote the  $m \times m$  identity and zero matrices, respectively. Noting that the only assumptions on the solution of (3) are its unique existence and continuous differentiability, the solution to (7) can also solve (3) for some suitable choice of piecewise continuous bounded  $u(\cdot)$ .

Certainly, determining the exact value of such function  $u\left(\cdot\right)$  is not possible in the presence of measurement noise and with limited number of observed data points. Yet, a proper estimate of  $u\left(\cdot\right)$  can be obtained by minimizing the quadratic cost

$$J = \int_{0}^{T} \beta \|u(t)\|^{2} dt + \sum_{n=0}^{N} w_{n} \|Cz(t_{n}) - y_{n}\|^{2}$$
 (8)

with respect to  $u\left(\cdot\right)$  and the initial state  $z\left(0\right)=z_0$  of (7a). In this quadratic cost functional,  $\beta$  is a positive constant and  $w_n$  for  $n=0,1,2,\ldots,N$  are nonnegative constants summing up to 1. The integral on the right-hand side of (8) penalizes a large second derivative  $u\left(t\right)$  to keep  $x\left(t\right)$  smooth and  $u\left(t\right)$  bounded, while the sum term penalizes large deviations of  $x\left(t\right)$  from the data points  $y_0,y_1,\ldots,y_N$  to keep it close to the empirically observed trajectory. By varying the regularization parameter  $\beta$ , a trade-off is made between the smoothness of  $x\left(t\right)$  and the goodness of ft, while the values of  $w_0,w_1,\ldots,w_N$  determine the relative importance of the ftting error at each point  $y_n$ .

After minimizing the cost functional (8) subject to the statespace equation (7a), the estimators

$$\hat{x}(t) = Cz^*(t), \quad t \in [0, T]$$

$$\hat{f}(\hat{x}(t)) = Dz^*(t), \quad t \in [0, T]$$

are obtained in terms of the optimal state trajectory  $z^*(t)$ . The matrix D in the second equation is defined as  $D = \begin{bmatrix} 0_m & I_m \end{bmatrix}$ .

The least squares estimation problem involving (7) and (8) is extendable to the case that the vector feld  $f(\cdot)$  in (3) is not only continuous, but also continuously differentiable. This new assumption implies that the second derivative  $\ddot{x}(t)$  exists and is continuous. To enforce the continuity of  $\ddot{x}(t)$ , the statespace equation (7) is redefined with the new vectors

$$z\left(t\right) = \begin{bmatrix} x^{T}\left(t\right) & \dot{x}^{T}\left(t\right) & \ddot{x}^{T}\left(t\right) \end{bmatrix}^{T}, \quad u\left(t\right) = \dddot{x}\left(t\right)$$
 (9)

and accordingly redefined parameters A, B, C, and D. Then, the least squares problem is redefined subject to this new state-space equation and a cost functional of the same structure (8). Depending on the prior knowledge on the smoothness of the vector  $\mathbf{f}$  eld  $f(\cdot)$ , this procedure is extendable to higher orders.

#### C. Selection of the Weighting Parameters

In a typical experiment, samples of the f ow curves are taken uniformly in time, that leads to nonuniform sampling in space as a result of temporal variations in  $\|\dot{x}(t)\|$ . This phenomenon results in nonuniform distribution of the data points along the f ow curves. Hence, for a fair distribution of f tting error along these curves, this error must be emphasized at the points with more sparse distribution of the data points, and deemphasized

for the points with more dense distribution. A straightforward approach to this problem is to take the weighting parameter  $w_n$  proportional to the empirical value of  $\|\dot{x}(t_n)\|$  estimated as the numerical differential  $\dot{y}_n$  in (5). Since the sequence  $\{\dot{y}_n\}_{n=0}^N$  is typically rough, it can be smoothed before generating  $w_n$ .

Selection of the regularization parameter  $\beta > 0$  in this work relies on human effort by direct investigation of the estimated trajectories of  $\hat{x}(t)$  and  $\hat{f}(\hat{x}(t))$ . Automated selection of this parameter has been proposed by cross-validation methods [39].

D. Conversion to a Linear Quadratic Tracking Problem

The cost functional (8) can be expressed as

$$J = \int_{0}^{T} \left( w(t) \|Cz(t) - y(t)\|^{2} + \beta \|u(t)\|^{2} \right) dt + w_{N} \|Cz(T) - y_{N}\|^{2}, \quad (10)$$

where y(t) is any continuous function satisfying  $y(t_n) = y_n$  for n = 0, 1, 2, ..., N - 1, and w(t) is defined as

$$w(t) = \sum_{n=0}^{N-1} w_n \delta(t - t_n)$$

in terms of the Dirac delta function  $\delta(\cdot)$ . With this new form of J, the problem of minimizing (8) with respect to the control trajectory u(t),  $t \in [0, T]$  and the initial state  $z_0$  of (7) reduces to an LQT problem and a simple quadratic optimization. The solution to the LQT problem can be accessed in any standard optimal control textbook such as [21], which is specialized in the remainder of this section for the cost functional (10).

For any f xed initial state  $z_0$  of the state-space equation (7), the minimum of (10) is a quadratic function of  $z_0$  given by

$$J^*(z_0) = J_0^* + 2q^T(0)z_0 + z_0^T P(0)z_0,$$

where  $J_0^*$  is a constant independent of  $z_0$ , and  $q\left(0\right)$  and  $P\left(0\right)$  are respectively a vector and an invertible matrix of appropriate dimensions. Then, the minimum of (10) over all initial states is attained by the specific choice

$$z_0^* = -P^{-1}(0) q(0).$$
 (11)

(12b)

The numerical values of P(0) and q(0) are determined by solving the set of differential equations

$$\dot{P}(t) = -A^{T}P(t) - P(t)A + \beta^{-1}P(t)BB^{T}P(t) - w(t)C^{T}C$$
(12a)  
$$\dot{q}(t) = -(A - \beta^{-1}BB^{T}P(t))^{T}q(t) + w(t)C^{T}y(t)$$

backward in time with the terminal condition

$$P(T) = w_N C^T C, \quad q(T) = -w_N C^T y_N.$$

By resolving this set of equations, the values of P(0) and q(0) are determined at t=0, from which, the optimal initial state is extracted according to (11), Moreover, in terms of the recorded trajectories of q(t) and P(t) over  $t \in [0,T]$ , the optimal state trajectory  $z^*(t)$ ,  $t \in [0,T]$  is given by the forward solution of

$$\dot{z}^*(t) = (A - \beta^{-1}BB^T P(t)) z^*(t) - \beta^{-1}BB^T q(t)$$
$$z^*(0) = z_0^*.$$

Considering the explicit form of w(t) involving Dirac delta functions, the set of differential equations (12) reduces to

$$\dot{P}(t) = -A^T P(t) - P(t) A + \beta^{-1} P(t) B B^T P(t)$$
$$\dot{q}(t) = -\left(A - \beta^{-1} B B^T P(t)\right)^T q(t)$$

over the intervals  $t \in (t_{n-1}, t_n]$  for  $n = N, N - 2, \dots, 2, 1$ . Moreover, the terminal condition for solving these equations over the interval  $(t_{n-1}, t_n]$  is determined in terms of the initial condition of the previous interval  $(t_n, t_{n+1}]$  according to

$$P(t_n) = P(t_n^+) + w_n C^T C$$
$$q(t_n) = q(t_n^+) - w_n C^T y_n.$$

These latter equations hold for  $n = N - 1, N - 2, \dots, 2, 1$  to obtain the terminal conditions, and for n = 0 to determine the actual values of P(0) and q(0).

# E. Nearest Neighbour Interpolation

Once the vector f eld  $f(\cdot)$  is estimated along L f ow curves

$$\hat{x}_{i}(t)$$
,  $\hat{f}(\hat{x}_{i}(t))$ ,  $t \in [0, T_{i}]$ ,  $i = 1, 2, ..., L$ , (13)

it is interpolated for those points  $x \in \mathbb{R}^m$  not lying on any of these curves. For any such  $x \in \mathbb{R}^m$ , define

$$d_{i}(x) = \min_{t \in [0, T_{i}]} \|\hat{x}_{i}(t) - x\|, \quad i = 1, 2, \dots, L$$
  
$$t_{i}^{*}(x) = \arg\min_{t \in [0, T_{i}]} \|\hat{x}_{i}(t) - x\|, \quad i = 1, 2, \dots, L.$$

Let  $1 \leq K \leq L$  be an integer. Among  $d_i(x)$ , i = 1, 2, ..., L, choose K with the smallest values and gather their indices in a set  $S_K(x)$ . Then, the K-nearest neighbour estimate of  $f(\cdot)$  at any point x not lying on any trajectory (13) is expressed as

$$\hat{f}_{K}\left(x\right) = \frac{\sum_{i \in \mathcal{S}_{K}\left(x\right)} d_{i}^{-1}\left(x\right) \hat{f}\left(\hat{x}_{i}\left(t_{i}^{*}\left(x\right)\right)\right)}{\sum_{i \in \mathcal{S}_{K}\left(x\right)} d_{i}^{-1}\left(x\right)} \,.$$

#### IV. ESTIMATION RESULTS FOR SIMULATED DATA

Before applying the least squares estimator of Section III to empirical data, its performance is evaluated for simulated data. Since for a simulated data set, the exact solution of (3) and its derivative are known, they can serve as a reference to evaluate the estimation performance. Moreover, the selection process of the regularization parameter  $\beta$  and the advantage of the triple integral formulation (9) over its double integral counterpart (6) are demonstrated using the simulated data.

For the purpose of simulations, the vector feld  $f(\cdot)$  in (3) was considered as the linear function

$$f(x) = \begin{bmatrix} -2 & -4 \\ 4 & -2 \end{bmatrix} x$$

with the initial state  $x_0=(3,-2)$ . The solution to the resulting state-space equation was numerically computed over  $t\in[0,1]$ . This solution was then sampled with a constant period 0.01 to generate the observation set (4) with a white Gaussian noise  $v_n$  of the covariance matrix diag (0.0004,0.0004). The resulting observation set is illustrated in Fig. 2(a).

Using the least squares method of Section III, the simulated state vector and its derivative were reconstructed with the triple

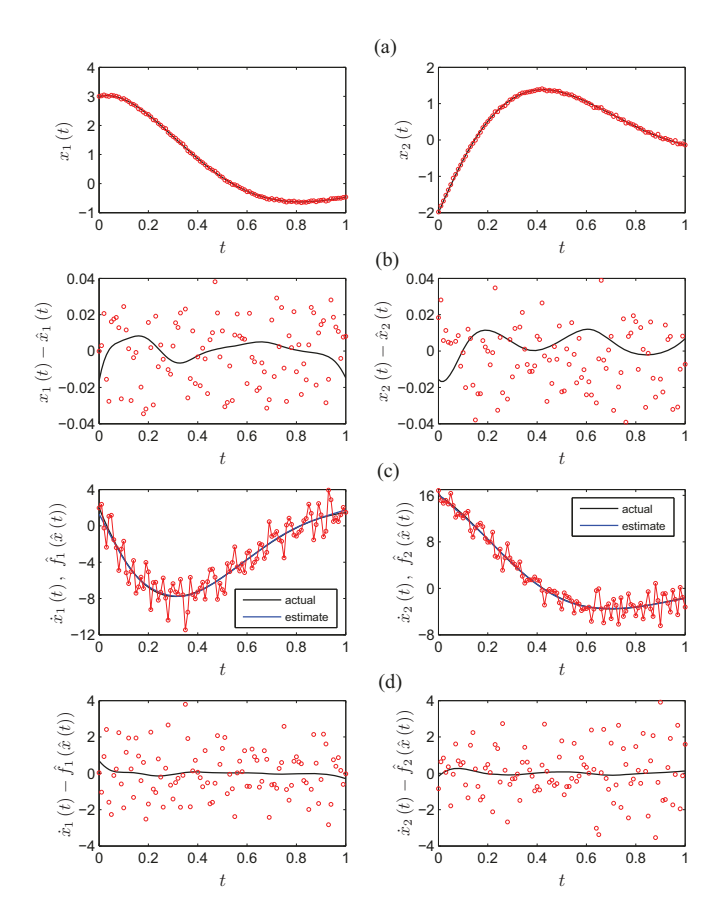


Fig. 2. Reconstruction of noisy simulated trajectories: (a) elements of the state vector versus time (solid lines) and their noisy measurements (markers); (b) estimation error of the state vector (solid lines) and the measurement noise (markers); (c) derivative of the state vector (dark solid lines), its least squares estimation (light solid lines), and the numerical differential (5) (markers); (d) estimation error of the derivative of state for the least squares method (solid lines) and for the numerical differentiation (markers).

integral model (9), the regularization parameter  $\beta=10^{-8}$ , and the weighting parameters  $w_n$  described in Section III-C. The reconstruction results are illustrated in Fig. 2. The estimation error of the state vector is illustrated versus time (solid lines) in Fig. 2(b), which shows signif cant improvement compared to the measurement noise (markers). Note that the latter is the estimation error in case the observed values are taken without further processing as the estimation of state. In Fig. 2(c), the derivative of the state vector (dark solid lines), its least squares estimation (light solid lines), and the numerical differential (5) (markers) are illustrated versus time. The effectiveness of the proposed least squares estimation method is best demonstrated by Fig. 2(d), which shows great improvement in the estimation error of derivative over the naive numerical differentiation (5).

The selection process for the regularization parameter  $\beta$  is explained in Fig. 3. This f gure illustrates the estimation of the derivative  $\dot{x}(t)$  for different values of  $\beta$  (only the f rst element is shown for simplicity). Certainly, decreasing the value of this parameter improves the goodness of ft, which is desirable; but its gradual decrease must be stopped whenever the f rst sign of overf tting emerges. This sign is manifested by the oscillatory behavior of the estimated trajectories in Fig. 3 for the values of  $\beta$  taken below  $\beta = 10^{-8}$ . Note that as  $\beta \to 0$ , the estimated

trajectory tends to the rough trajectory generated by numerical differentiation using (5).

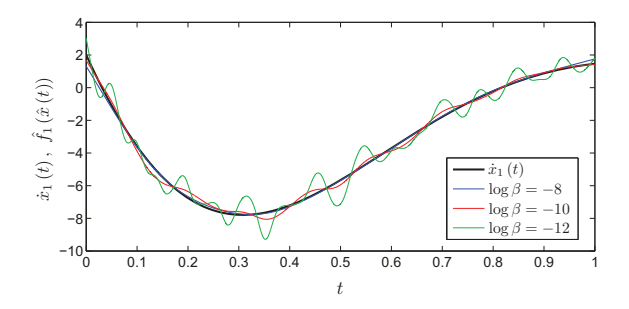


Fig. 3. Selection of the regularization parameter  $\beta$ . The oscillatory behavior observed for  $\beta < 10^{-8}$  is a sign of overfitting, which must be prevented.

Fig. 4 compares the estimation performance for two models of double integral in (6) and triple integral in (9). In this f gure, the f rst element  $\dot{x}_1$  (t) of the state derivative, together with its estimation based on both models are illustrated. The best value of the regularization parameter  $\beta$  for the double integral model was selected as  $\beta = 10^{-5}$ . Even with this best value of  $\beta$ , the triple integral model noticeably outperforms its double integral counterpart, particularly at the endpoints of the trajectory.

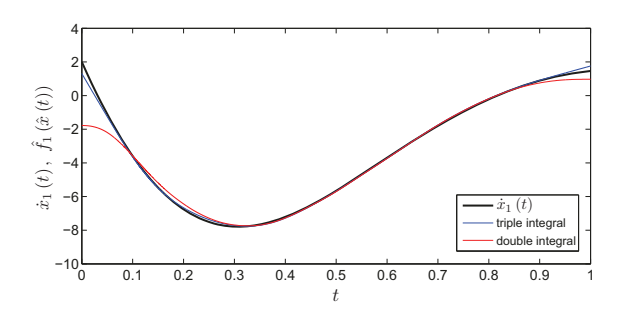


Fig. 4. Performance comparison between the double integral model (6) with its triple integral counterpart (9).

# V. EXPERIMENTAL MODELING OF MAGNETIC FORCE

The reconstruction method of Section III was implemented on MATLAB to reconstruct the magnetic force f eld around a NdFeB cubic permanent magnet of side length 15.9 mm. The reconstruction procedure utilized the triple integral formulation in (9) with the regularization parameter  $\beta=10^{-13}$ . To obtain the weighting parameters  $w_n$ , the sequence  $\dot{y}_0, \dot{y}_1, \ldots, \dot{y}_N$  of numerical differentials was computed from (5) and was then smoothed using a weighted moving average f lter implemented by a Hamming window of length 21. The lengths of L=17 recorded data sets were ranging from N=858 to N=4376, corresponding to experiment times T=1.32 to T=6.63 sec. The reconstruction results for a typical trajectory are illustrated in Figs. 5(a) through 5(c).

After reconstruction of L=17 individual trajectories (13), the entire magnetic force was reconstructed using the nearest neighbour interpolation scheme of Section III-E with K=6. Due to the geometric symmetry of the magnet, it is known in advance that its magnetic force is symmetric with respect to the x-axis in the coordinate system of Fig. 1(c). Therefore, the

symmetric images of the reconstructed curves were included in the dictionary (13) to both improve the interpolation resolution using 2L = 34 trajectories, and to preserve the symmetry of the reconstructed vector f eld shown in Figs. 5(d) through 5(f).

#### VI. CONCLUSION

A least squares estimation method combined with a nearest neighbour interpolation scheme was developed to reconstruct vector f elds from their empirically recorded f ow curves. As a case study, the reconstruction scheme was applied to empirical data to build an experimental model for a magnetic force f eld. The reconstruction accuracy can be improved by involving the spatial correlation of the nearby data points into the estimation problem, which is planned for future work.

#### REFERENCES

- [1] C. Gosse and V. Croquette, "Magnetic tweezers: Micromanipulation and force measurement at the molecular level," *Biophysical Journal*, vol. 82, no. 6, pp. 3314–3329, 2002.
- [2] M. B. Khamesee, N. Kato, Y. Nomura, and T. Nakamura, "Design and control of a microrobotic system using magnetic levitation," *IEEE/ASME Trans. Mechatronics*, vol. 7, no. 1, pp. 1–14, 2002.
- [3] M. Sendoh, K. Ishiyama, and K.-I. Arai, "Fabrication of magnetic actuator for use in a capsule endoscope," *IEEE Trans. Magn.*, vol. 39, no. 5, pp. 3232–3234, 2003.
- [4] A. Komaee and B. Shapiro, "Steering a ferromagnetic particle by magnetic feedback control: Algorithm design and validation," in *Proc. of* 2010 American Control Conference (ACC 2010), pp. 6543–6548, 2010.
- [5] M. P. Kummer, J. J. Abbott, B. E. Kratochvil, R. Borer, A. Sengul, and B. J. Nelson, "OctoMag: An electromagnetic system for 5-DOF wireless micromanipulation," *IEEE Trans. Robot.*, vol. 26, no. 6, pp. 1006–1017, 2010.
- [6] M. Simi, P. Valdastri, C. Quaglia, A. Menciassi, and P. Dario, "Design, fabrication, and testing of a capsule with hybrid locomotion for gastrointestinal tract exploration," *IEEE/ASME Trans. Mechatronics*, vol. 15, no. 2, pp. 170–180, 2010.
- [7] R. Probst, J. Lin, A. Komaee, A. Nacev, Z. Cummins, and B. Shapiro, "Planar steering of a single ferrof uid drop by optimal minimum power dynamic feedback control of four electromagnets at a distance," *J MAGN MATER*, vol. 323, no. 7, pp. 885–896, 2011.
- [8] A. Komaee and B. Shapiro, "Magnetic steering of a distributed ferrof uid spot towards a deep target with minimal spreading," in *Proc. of 50th IEEE Conference on Decision and Control and European Control Conference*, pp. 7950–7955, Dec. 2011.
- [9] A. Komaee and B. Shapiro, "Steering a ferromagnetic particle by optimal magnetic feedback control," *IEEE Trans. Control Syst. Technol.*, vol. 20, no. 4, pp. 1011–1024, 2012.
- [10] S. Yim and M. Sitti, "Design and rolling locomotion of a magnetically actuated soft capsule endoscope," *IEEE Trans. Robot.*, vol. 28, no. 1, pp. 183–194, 2012.
- [11] A. Nacev, A. Komaee, A. Sarwar, R. Probst, S. H. Kim, M. Emmert-Buck, and B. Shapiro, "Towards control of magnetic fuids in patients: directing therapeutic nanoparticles to disease locations," *IEEE Control Syst. Mag.*, vol. 32, no. 3, pp. 32–74, 2012.
- [12] A. Komaee, R. Lee, A. Nacev, R. Probst, A. Sarwar, D. A. Depireux, K. J. Dormer, I. Rutel, and B. Shapiro, *Magnetic Nanoparticles: From Fabrication to Clinical Applications*, ch. Putting Therapeutic Nanoparticles Where They Need to Go by Magnet Systems Design and Control, pp. 419–448. CRC Press, 2012.
- [13] M. Beccani, C. Di Natali, L. J. Sliker, J. A. Schoen, M. E. Rentschler, and P. Valdastri, "Wireless tissue palpation for intraoperative detection of lumps in the soft tissue," *IEEE Trans. Biomed. Eng.*, vol. 61, no. 2, pp. 353–361, 2014.
- [14] H. Marino, C. Bergeles, and B. J. Nelson, "Robust electromagnetic control of microrobots under force and localization uncertainties," *IEEE Trans. Autom. Sci. Eng.*, vol. 11, no. 1, pp. 310–316, 2014.
- [15] V. Iacovacci, L. Ricotti, P. Dario, and A. Menciassi, "Design and development of a mechatronic system for noninvasive ref lling of implantable artificial pancreas," *IEEE/ASME Trans. Mechatronics*, vol. 20, no. 3, pp. 1160–1169, 2015.

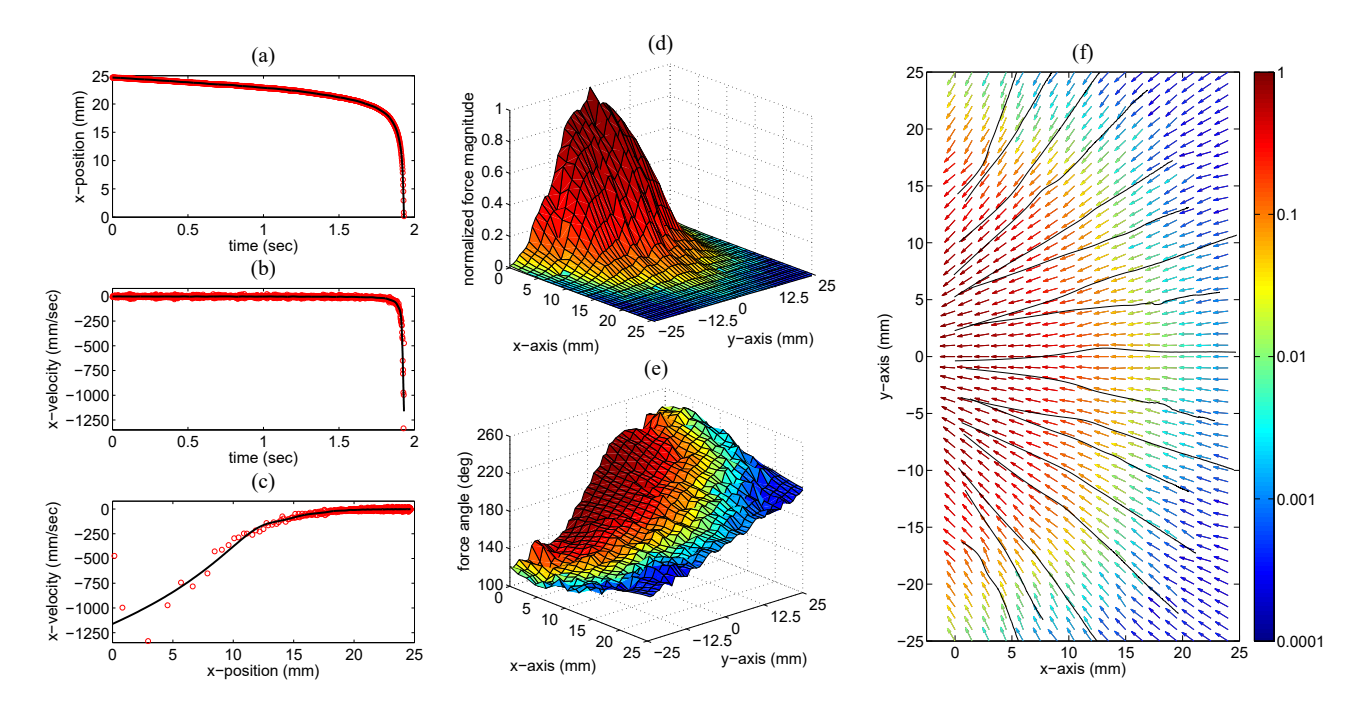


Fig. 5. Reconstruction of magnetic force. (a) The x-component of a typical trajectory of motion (solid line) reconstructed from observed data (markers). (b) The x-component of the estimated derivative (velocity) of the same trajectory (solid line), and the numerical differentials  $\dot{y}_n$  determined from (5) (markers). (c) The x-component of velocity [proportional to the magnetic force by (2)] versus distance from the face of magnet along x-axis. The markers represent the x-component of  $\dot{y}_n$  against the x-component of  $y_n$ . (d) Normalized magnitude of the reconstructed magnetic force for the points on the plane of motion. The normalization factor is the maximum force at the face of the magnet. (e) Direction of the reconstructed magnetic force determined as the angle between x-axis and the magnetic force at each point. (f) Quiver plot of the reconstructed magnetic force. The force directions are represented by vectors of equal length, and the magnitude of force is color-coded with a logarithmic scale. The reconstructed trajectories of motion are shown in (f) by solid lines.

- [16] L. Sliker, G. Ciuti, M. Rentschler, and A. Menciassi, "Magnetically driven medical devices: a review," *Expert Review of Medical Devices*, vol. 12, no. 6, pp. 737–752, 2015.
- [17] A. Komaee, "Feedback control for transportation of magnetic fuids with minimal dispersion: A first step toward targeted magnetic drug delivery," *IEEE Trans. Control Syst. Technol.*, vol. 25, no. 1, pp. 129–144, 2017.
- [18] N. Riahi and A. Komaee, "Steering magnetic particles by feedback control of permanent magnet manipulators," in *Proc. of 2019 American Control Conference (ACC 2019)*, pp. 5432–5437, 2019.
- [19] N. Riahi, L. R. Tituaña, and A. Komaee, "Homotopy continuation for feedback linearization of noncontact magnetic manipulators," in *Proc. of* 2020 American Control Conference (ACC 2020), pp. 4295–4300, 2020.
- [20] N. Riahi and A. Komaee, "Noncontact steering of magnetic objects by optimal linear feedback control of permanent magnet manipulators," in Proc. of 2020 IEEE/ASME International Conference on Advanced Intelligent Mechatronics (AIM 2020), pp. 30–35, 2020.
- [21] D. E. Kirk, Optimal Control Theory: An Introduction. Englewood Cliffs, NJ: Prentice-Hall, 1970.
- [22] S. J. Norton, "Tomographic reconstruction of 2-D vector f elds: application to f ow imaging," *Geophysical Journal International*, vol. 97, no. 1, pp. 161–168, 1989.
- [23] H. Braun and A. Hauck, "Tomographic reconstruction of vector felds," IEEE Trans. Signal Process., vol. 39, no. 2, pp. 464–471, 1991.
- [24] S. J. Norton, "Unique tomographic reconstruction of vector felds using boundary data," *IEEE Trans. Image Process.*, vol. 1, no. 3, pp. 406–412, 1992
- [25] N. F. Osman and J. L. Prince, "Reconstruction of vector felds in bounded domain vector tomography," in *Proc. of International Con*ference on Image Processing, vol. 1, pp. 476–479, 1997.
- [26] A. Tamasan, "Tomographic reconstruction of vector felds in variable background media," *Inverse Problems*, vol. 23, no. 5, pp. 2197–2205, 2007.
- [27] T. Pf tzenreiter and T. Schuster, "Tomographic reconstruction of the curl and divergence of 2D vector f elds taking refractions into account," SIAM Journal on Imaging Sciences, vol. 4, no. 1, pp. 40–56, 2011.
- [28] C. Donnelly, S. Gliga, V. Scagnoli, M. Holler, J. Raabe, L. J. Heyderman, and M. Guizar-Sicairos, "Tomographic reconstruction of a three-dimensional magnetization vector feld," *New Journal of Physics*, vol. 20, no. 8, p. 083009, 2018.

- [29] G. Gouesbet, "Reconstruction of vector felds: the case of the lorenz system," *Physical Review A*, vol. 46, no. 4, pp. 1784–1796, 1992.
- [30] B. P. Bezruchko and D. A. Smirnov, "Constructing nonautonomous differential equations from experimental time series," *Physical Review* E, vol. 63, no. 1, p. 016207, 2000.
- [31] P. Perona, A. Porporato, and L. Ridolf, "On the trajectory method for the reconstruction of differential equations from time series," *Nonlinear Dynamics*, vol. 23, no. 1, pp. 13–33, 2000.
- [32] T. Johnson and W. Tucker, "Rigorous parameter reconstruction for differential equations with noisy data," *Automatica*, vol. 44, no. 9, pp. 2422–2426, 2008.
- [33] S. Chen, A. Shojaie, and D. M. Witten, "Network reconstruction from high-dimensional ordinary differential equations," *Journal of the American Statistical Association*, vol. 112, no. 520, pp. 1697–1707, 2017.
- [34] E. Kaiser, J. N. Kutz, and S. L. Brunton, "Sparse identification of nonlinear dynamics for model predictive control in the low-data limit," *Proceedings of the Royal Society A*, vol. 474, no. 2219, p. 20180335, 2018.
- [35] S. Zhang and G. Lin, "Robust data-driven discovery of governing physical laws with error bars," *Proceedings of the Royal Society A*, vol. 474, no. 2217, p. 20180305, 2018.
- [36] M. Quade, M. Abel, J. Nathan Kutz, and S. L. Brunton, "Sparse identification of nonlinear dynamics for rapid model recovery," *Chaos: An Interdisciplinary Journal of Nonlinear Science*, vol. 28, no. 6, p. 063116, 2018.
- [37] K. Champion, B. Lusch, J. N. Kutz, and S. L. Brunton, "Data-driven discovery of coordinates and governing equations," *Proceedings of the National Academy of Sciences*, vol. 116, no. 45, pp. 22445–22451, 2019.
- [38] M. Stender, S. Oberst, and N. Hoffmann, "Recovery of differential equations from impulse response time series data for model identification and feature extraction," *Vibration*, vol. 2, no. 1, pp. 25–46, 2019.
- [39] B. Dey and P. S. Krishnaprasad, "Trajectory smoothing as a linear optimal control problem," in Proc. of 50th Annual Allerton Conference on Communication, Control, and Computing (Allerton 2012), pp. 1490– 1497, 2012.
- [40] H. K. Khalil, Nonlinear Systems. Upper Saddle River: Prentice-Hall, Inc., 2002.